

Heterogeneity of the action potential duration is required for sustained atrial fibrillation

Uma Mahesh R. Avula, ... , Steven O. Marx, Elaine Y. Wan

JCI Insight. 2019. <https://doi.org/10.1172/jci.insight.128765>.

Research

In-Press Preview

Cardiology

Cell biology

Atrial fibrillation (AF) is the most common cardiac arrhythmia and accounts for substantial morbidity and mortality. Recently, we created a mouse model with spontaneous and sustained AF caused by a mutation in the $Na_v1.5$ channel (F1759A) that enhances persistent Na^+ current, thereby enabling the investigation of molecular mechanisms that cause AF and the identification of novel treatment strategies. The mice have regional heterogeneity of action potential duration of the atria similar to observations in patients with AF. In these mice, we found that the initiation and persistence of the rotational reentrant AF arrhythmias, known as spiral waves or rotors, were dependent upon action potential duration heterogeneity. The centers of the rotors were localized to regions of greatest heterogeneity of the action potential duration. Pharmacologically attenuating the action potential duration heterogeneity reduced both spontaneous and pacing-induced AF. Computer-based simulations also demonstrated that the action potential duration heterogeneity is sufficient to generate rotors that manifest as AF. Taken together, these findings suggest that action potential duration heterogeneity in mice and humans is one mechanism by which AF is initiated and that reducing action potential duration heterogeneity can lessen the burden of AF.

Find the latest version:

<http://jci.me/128765/pdf>



Heterogeneity of the action potential duration is required for sustained atrial fibrillation

Uma Mahesh R. Avula¹, Jeffrey Abrams¹, Alexander Katchman¹, Sergey Zakharov¹, Sergey Mironov², Joseph Bayne¹, Daniel Roybal¹, Anirudh Gorti¹, Lin Yang¹, Vivek Iyer³, Marc Waase¹, Deepak Saluja¹, Edward J. Ciaccio¹, Hasan Garan¹, Andrew R. Marks^{4,5}, Steven O. Marx^{1,a} and Elaine Y. Wan^{1,a}

¹ Division of Cardiology, Department of Medicine, Vagelos College of Physicians and Surgeons, Columbia University, New York, New York 10032. ² Center for Arrhythmia Research, Division of Cardiology, University of Michigan, Ann Arbor, MI 48109. ³ Marin General Hospital, Greenbrae, CA 94904. ⁴ The Wu Center for Molecular Cardiology, Columbia University, New York, NY 10032. ⁵ Department of Physiology and Cellular Biophysics, Vagelos College of Physicians and Surgeons, Columbia University, New York, NY 10032

Running title: Action potential duration heterogeneity promotes atrial fibrillation

^a Address correspondence to:

Elaine Wan, M.D.
622 W168 Street, PH 3-Center
New York, NY 10032
eyw2003@cumc.columbia.edu
Tel: (212) 342-0400; Fax: (212) 342-1992

or

Steven O. Marx, M.D.
622 W168th Street, PH-3 Center
New York, NY 10032
sm460@cumc.columbia.edu
Tel: (212) 305-0271; Fax: (212) 342-3121

Keywords: atrial fibrillation, optical mapping, action potential duration, sodium channel, heart

ABSTRACT

Atrial fibrillation (AF) is the most common cardiac arrhythmia and accounts for substantial morbidity and mortality. Recently, we created a mouse model with spontaneous and sustained AF caused by a mutation in the Nav1.5 channel (F1759A) that enhances persistent Na⁺ current, thereby enabling the investigation of molecular mechanisms that cause AF and the identification of novel treatment strategies. The mice have regional heterogeneity of action potential duration of the atria similar to observations in patients with AF. In these mice, we found that the initiation and persistence of the rotational reentrant AF arrhythmias, known as spiral waves or rotors, were dependent upon action potential duration heterogeneity. The centers of the rotors were localized to regions of greatest heterogeneity of the action potential duration. Pharmacologically attenuating the action potential duration heterogeneity reduced both spontaneous and pacing-induced AF. Computer-based simulations also demonstrated that the action potential duration heterogeneity is sufficient to generate rotors that manifest as AF. Taken together, these findings suggest that action potential duration heterogeneity in mice and humans is one mechanism by which AF is initiated and that reducing action potential duration heterogeneity can lessen the burden of AF.

INTRODUCTION

Atrial fibrillation (AF) is the most common cardiac arrhythmia, yet its mechanisms are still unclear and therapeutic options are limited. The development of AF is a complex process involving interplay between electrical and structural remodeling in the atria, autonomic imbalance, abnormal metabolism and genetic factors. In humans, genetic and acquired Na^+ channel dysfunctions have been associated with cardiomyopathy and electrical instability including AF (1-3). Aging, atrial stretch and fibrosis also alter the anatomical substrate by increasing persistent Na^+ current (4), thereby prolonging the action potential duration (APD) and subsequently triggering arrhythmogenesis. Drugs that reduce persistent Na^+ current are frequently used to treat patients with AF. Recently, we reported that increased persistent Na^+ current, caused by transgenic (TG) expression in mice of a gain-of-function mutant human $\text{Nav}1.5$ channel, was sufficient to cause an atrial cardiomyopathy and prolonged episodes of spontaneous AF (5).

In humans, the initiation of AF is frequently triggered by increased automaticity within the myocardial sleeves of pulmonary veins. However, isolating the pulmonary veins by ablation is often not curative since AF can also be initiated by triggers outside the pulmonary veins, for example within the posterior atrial wall (6). The discovery of electrical rotational activity in the atria, called rotors or spiral waves, shown using high-resolution optical mapping in animal models of AF, and activation mapping in humans using multi-electrode intra-atrial basket catheters (7) and body surface electrograms has driven new ablative therapeutic approaches. However, the question still remains: why do rotors occur where they occur?

Atrial fibrosis has been proposed as one mechanism for rotor clustering and whereas a correlation between the amount of late gadolinium enhancement detected by MRI and the number of regions exhibiting re-entry has been shown (8), other studies have found no such correlation (9,

10). A role for APD heterogeneity in the genesis of rotors has been shown in in vitro cell culture studies of virally-transduced neonatal rat ventricular myocyte monolayers variably expressing the hERG protein. The predominant areas of rotational activity and wavebreaks were in border zones of enhanced APD dispersion (11). Computer simulations have shown that areas of long-short APD alternation adjacent to areas with short-long APD alternation increase dispersion and refractoriness, leading to wave break and initiation of reentry, explaining the progression from sinus rhythm or rapid tachycardia to AF (12, 13). These conclusions have yet to be tested in vivo because a limitation of both large and small animal models of AF is the inability to recapitulate the spontaneity and long duration of AF seen in humans. Previous studies in rabbits have shown APD difference between the right and left atria, however they have not looked at APD dispersion within one atrium with any cardiac disease or arrhythmia (14).

Herein, we show that in a mouse model of spontaneous AF, rotors and reentrant waves are dependent on atrial APD heterogeneity and are anchored to regions where the APD dispersion is greatest. Using a monophasic action potential (MAP) contact catheter (15), we show that spatial APD heterogeneity is similarly present in the posterior left atrial wall of patients with paroxysmal or persistent AF. Attenuating the atrial APD heterogeneity reduces spontaneous and pacing-induced AF re-induction in mice. Taken together, these in vivo and in silico studies (16) suggest that spatial APD dispersion is one mechanism by which AF is initiated and can anchor rotational reentry.

RESULTS

Wavebreaks and reentrant waves in AF mice

The AF mice were generated by crossing mice with FLAG-tagged F1759A human *SCN5A* (Nav_v1.5) fused to a modified murine α -myosin heavy chain, tetracycline-inducible promoter vector (17), and mice with cardiac-specific expression of reverse tetracycline-controlled transactivator protein (rtTA) (18). Without doxycycline, the double transgenic (dTG) mice developed structural alterations including atrial and ventricular enlargement, myofibril disarray, fibrosis, mitochondrial necrosis, and electrophysiological dysfunctions leading to spontaneous and prolonged episodes of AF (5) (Figure 1A). The expression of the F1759A-Nav_v1.5 channels in the absence of doxycycline is likely due to a low basal binding of rtTA protein to the *Tet* operator sequences (so called “leak”) (18). Not only did the F1759A mutation (19) enable us to distinguish the functional characteristics of the transgenic Na⁺ channels, which are relatively resistant to local anesthetics such as lidocaine, from endogenous channels, but also prevented complete inactivation of Nav_v1.5, resulting in a persistent Na⁺ current.

Epicardial surface optical voltage mapping of the anterior surface of Langendorff-perfused F1759A-dTG hearts revealed a variety of activation patterns including a single dominant clockwise or counterclockwise rotor, figure of 8 reentry, multiple rotors in either atrium or both atria, and multiple wavebreaks with fibrillatory conduction (Figure 1B, Supplemental Figure 1A). Rotors are spiral waves with patterns of circular reentry for one or more cycles. AF persisted with the same arrhythmic mechanisms (rotors and/or wavebreaks) during extended recordings of up to 1 hour. Conduction velocity and the dispersion of the conduction velocity were not significantly altered in the TG mice compared to littermate controls (Supplemental Figure 1B-G).

To elucidate the underlying electrophysiologic substrate, the Langendorff-perfused hearts were perfused with a hyperkalemic solution to terminate the arrhythmias. Thereafter, a normokalemic solution was infused and the atrial APD was measured by pacing the atria at 10-Hz (Figure 1C-D). The maximal and mean APD were increased by ~ 2-fold in both right and left atria of the F1759A-dTG mice compared to control mice (Figure 1E). Consistently, we observed APD heterogeneity in both left and right atria – demonstrated by the non-uniformity in APD maps (Figure 1C) and in all-point histograms of the APD (Figure 1F). The dispersion of APD, assessed by both the difference between greatest and least APD (Figure 1G), and the coefficient of variation of APD (Supplemental Figure 1F-G) were significantly greater in the F1759A-dTG mice compared to littermate control mice.

Heterogeneity of action potential duration in patients with atrial fibrillation

Does spatial heterogeneity of the APD exist in patients with AF? Prior recordings of MAPs studies in humans demonstrated that alternans of the APD is a dynamic substrate for AF (20). We acquired electro-anatomical voltage maps and MAPs in sinus rhythm in 5 patients with paroxysmal or persistent AF and normal left ventricular function. The patients ranged in age from 35 to 85 with a mean of 62.4 ± 8.4 years, 80% were men, BMI was 28.5 ± 3.4 kg/m², and LA diameter was 3.9 ± 0.2 cm. In patients #1, #3, #4 and #5 electro-anatomical voltage mapping revealed little to mild scarring of the posterior wall, whereas patients #2, 4 and 5 showed scarring within the pulmonary veins (Figure 1H). We selected 4-6 regions without scar in each patient to measure the APD at 90% repolarization during atrial pacing at a cycle length of 500 ms (120 beats per minute). The dispersion of APD in the five patients, assessed by the difference between the greatest and least APD, was 39, 55, 56, 57, and 70 ms respectively. We were unable to perform similar mapping studies on control patients without a history of atrial arrhythmias due to IRB restrictions. Although

we cannot exclude the possibility that similar heterogeneity is present in patients without AF, the most conservative interpretation of the human findings is that heterogeneity of the APD exists in patients with AF, perhaps enabling the sustenance of AF. Using our mouse model of AF, we sought to identify the role of heterogeneity of AF in the initiation and perpetuation of AF.

Spatial APD gradients are a substrate for reentry, rotors and wavebreaks

Using both anti-FLAG immunocytochemistry (Figure 2A-B) and patch clamp (Figure 2C-F) analyses of isolated atrial cardiomyocytes, we found that expression of the FLAG-epitope-tagged-F1759A mutant Nav_v1.5 channels varied from cell-to-cell in the F1759A-dTG mice. Some myocytes had no lidocaine-resistant Na⁺ current, whereas others had more than 60% resistant current (Figure 2C-D). The F1759A mutation prevented complete inactivation of Nav_v1.5, thereby increasing persistent Na⁺ current in atrial cardiomyocytes isolated from F1759A-dTG mice (Figure 2E). Although the F1759A-Nav_v1.5 channels are relatively resistant to ranolazine, the persistent Na⁺ current is readily inhibited by superfusion of 500 μM ranolazine (Figure 2E). Similar to and directly correlated with the variation in lidocaine-resistant Na⁺ current density, we observed marked variation in the amount of persistent Na⁺ current caused by variable cell-to-cell expression of F1759A-Nav_v1.5 channels in atrial cardiomyocytes (Figure 2F). The cell-to-cell variation in expression of the F1759A-Nav_v1.5 channels in the absence of doxycycline is likely due to variations in the leakiness of the *Tet* promoter in the atrial myocytes.

Why are rotors and wavebreaks anchored in specific regions of the atria and what, if any, electrophysiological restraints dictate the meandering boundaries? The core of the rotor, known as singularity points, and areas of wavebreaks were quantified by plotting the singularity points over time and creating singularity point density (SPD) maps for both spontaneous AF and for AF that was re-initiated either spontaneously or by burst-pacing after hyperkalemia-induced conversion.

The trajectories of the singularity points then were superimposed on 2-dimensional and 3-dimensional projections of the APD₅₀ map acquired in sinus rhythm. For both spontaneous and re-initiated AF, the trajectory of the rotor's core meandered but was tightly delimited within the regions of high APD gradients (Figure 3A-B; Supplemental Figure 2A-B). Similar patterns were observed in hearts with a dominant rotor (Supplemental Video 1) and hearts with multiple wavebreaks (Supplemental Video 2) in the atria. In 10 of 11 mice with spontaneous AF, the APD dispersion and the density of singularity points were positively and significantly correlated (Figure 3C) with a mean slope of 4.0 ± 0.7 singularity points per ms of APD dispersion ($P < 0.0001$).

In regions with a high density of singularity points, the mean APDs were increased by ~2-fold (Figure 3D), and the APD dispersion was increased by ~3-4-fold in the atria of F1759A-dTG mice as compared to similar locations in littermate control mice (Figure 3E). The APD dispersion within regions of high density of singularity points, determined by subtracting the maximal and minimal APD values within the small 10 X 10 pixel box, was nearly as high as the dispersion throughout each atria. We quantified the dependence of rotor and wavebreak anchoring upon heterogeneity of APD by manually determining within multiple 10 X 10 pixel boxes the maximal APD dispersion and the density of singularity points during each of the 4096 frames of a 5-second optically-acquired movie. Overall, these findings imply that the singularity points of rotors and the regions of wavebreaks are anchored at regions of high APD gradients, specifically at the boundaries of long and short APD regions.

Minimizing spatial APD gradients reduces atrial fibrillation inducibility

Consistent with the thesis that increased APD causes early after-depolarizations (EADs) that can trigger arrhythmias, we observed using optically-acquired voltage maps and time space plots pacing-induced phase 3 EADs and rotors in the atria of the F1759A-dTG hearts (Figure 4A-D).

Previously, we showed that a single intraperitoneal injection of SEA-0400, an inhibitor of the Na⁺-Ca²⁺ exchanger, markedly reduced the burden of spontaneous AF in mice (5). We optically acquired voltage maps of Langendorff-perfused F1759A-dTG hearts before (vehicle) and after perfusion with SEA-0400. SEA-0400 did not significantly alter atrial APD or APD dispersion (Figure 4E-F), however the number of EADs and episodes of AF induced by EADs were markedly reduced (Figure 4G-I). Thus, the initiation and/or persistence of AF in this model requires the generation of EADs.

We also hypothesized that inhomogeneity of the atrial APD can form the substrate for initiating and sustaining atrial arrhythmias in these mice. We optically acquired voltage maps of Langendorff-perfused hearts before and after infusion of 500 μM ranolazine and 20 nM anemone toxin (ATX-II) (Figure 5A-C). Ranolazine was sufficient to reduce the APD by 30% ($P < 0.0001$) and APD dispersion by 50% ($P < 0.0001$) compared to vehicle-perfused hearts (Figure 5A-B, D). Ranolazine had potent anti-fibrillatory effects: whereas sustained AF was induced by 20-Hz pacing in 100% of vehicle-perfused hearts, none of the ranolazine-perfused hearts could be induced to AF (N=5 animals, $P = 0.008$ by Fisher's exact test). Although ranolazine markedly reduced the number of EADs (Figure 5E-F), likely predominantly accounting for the anti-arrhythmic effect, the likelihood of EADs causing AF was also completely reduced by ranolazine (Figure 5F). Ranolazine had minimal effects on conduction velocity (Supplemental Figure 3). Although an off-target effect of ranolazine is inhibition of hERG channels (21), these channels are not expressed in murine myocardium.

The converse approach for reducing APD dispersion is to increase the APD through the atria. Anemone toxin, which enhances persistent Na⁺ current (22), increased the mean atrial APD by 31% ($P < 0.0001$), but concomitantly reduced APD dispersion by 38% ($P < 0.001$) (Figure 5C-D).

Anemone toxin also had potent anti-fibrillatory effects: only 1 of 5 mice were inducible AF by 20-Hz burst pacing ($P=0.048$ by Fisher's exact test compared to control). The conduction velocity, however, was only minimally affected by anemone toxin (Supplemental Figure 3). Although anemone toxin did not reduce the frequency of EADs, the frequency of EADs triggering AF was markedly reduced (Figure 5F-G).

Next, we explored whether after-depolarizations in the substrate of normal APD and normal dispersion of APD could initiate and sustain AF in the F1759A-dTG hearts. Langendorff-perfused F1759A-dTG hearts were first treated with ranolazine, which normalized the APD and the dispersion of APD (Figure 5H-I). To increase after-depolarizations, we added $0.9\ \mu\text{M}$ digoxin, a $\text{Na}^+\text{-K}^+$ ATPase inhibitor, to the ranolazine-containing perfusate. Although digoxin had no effect on the APD or dispersion of the APD (Figure 5H-I), it markedly increased the number of after-depolarizations (Figure 5J-K), but these after-depolarizations failed to initiate or perpetuate AF in the presence of ranolazine (Figure 5L). Taken together, these findings demonstrate that spatial APD inhomogeneity is essential for initiating and sustaining AF caused by increased persistent Na^+ current.

Simulations demonstrate that spatial APD heterogeneity promotes atrial fibrillation

We used a previously described automaton (16) to test whether spatial APD heterogeneity is sufficient to perpetuate AF. In this simulation, we utilized two APD values, 100 and 130 ms, and induced fibrillatory activity by delivering premature S1-S2 stimulation. When the grid had a homogenous APD (Figure 5M, upper), extrastimuli did not produce any fibrillatory activity. In contrast, when the grid contained two APD regions with a soft boundary between the two, extrastimuli caused sustained rotors with the singularity point fixed at the boundary between the two APD regions (Figure 5M, lower; Supplemental Video 3). Thus, similar to previously

published modeling studies (11, 23, 24), we found that heterogeneity of the APD is sufficient to form a suitable substrate to perpetuate AF.

DISCUSSION

There are several lines of evidence supporting the relevance of this AF model and gain-of-function Nav1.5 abnormalities to AF in humans (25): (i) The incidence of AF is increased in LQT3 patients who harbor *SCN5A* mutations (26). (ii) Persistent Na⁺ current is increased by 26% in atrial appendages of patients with permanent AF (2). (iii) Ranolazine reduced atrial arrhythmias and new AF episodes in clinical trials (27, 28): (iv) Increased persistent Na⁺ current is observed in pathological conditions associated with an increased incidence of AF. Naturally, mouse models have limitations, especially in regards to repolarizing currents, reflecting the differences in the ion channel profiles responsible for repolarization in humans and mice. *Scn5a* mouse models of human *SCN5A* channelopathies, however, recapitulate many of the ECG and arrhythmia phenotypes observed in humans.

Increased anatomic and electrophysiological heterogeneity in the atrium due to structural changes such as fibrosis, chamber enlargement or electrophysiological dysfunctions are known to contribute to the pathogenesis of atrial arrhythmias in humans. Using a MAP contact catheter, we demonstrated that spatial APD heterogeneity is also present in patients with AF, similar to the APD heterogeneity we observed in the mouse model of AF. MAP recordings are technically challenging, and there is controversy regarding the cellular basis for MAPs (15, 29). It is unlikely, however, that the inhomogeneity of APD₉₀ measured by MAP contact electrode was artifactual, caused by catheter movement or variability in contact force, because the MAP signals were stable and of typical and consistent morphology. Is the inhomogeneity of the APD abnormal in patients

with AF? Due to IRB restrictions, we could not determine if inhomogeneity of the APD is also present in patients without AF. Some degree of dispersion may be present in the normal left atrium. It is conceivable that individuals without AF also have inhomogeneity of the APD, perhaps predisposing them to AF over time, especially if they develop diseases associated with increased early after-depolarizations (for example, heart failure). In rabbits without disease, for instance, variability in APD was observed between four regions of the atria (14).

Increased spatial dispersion of the APD in mice facilitated the initiation of AF by anchoring reentrant circuits at border zones of regions with high APD heterogeneity. Although EADs are an important trigger of arrhythmogenesis, EADs failed to initiate AF in the absence of APD heterogeneity. Our findings suggest that persistent Na^+ current-induced AF is dependent upon the presence of both EADs and atrial substrate heterogeneity. Computer simulation confirmed that APD heterogeneity is sufficient to sustain rotational re-entry upon premature stimulation, and to anchor the rotor's center within the boundaries of the APD gradient. It is unlikely that fibrosis, which is only modestly increased in the atria of F1759A-dTG mice, is the major driver of APD heterogeneity or anchoring of the rotors since the distribution of fibrosis is diffuse.

There are several limitations of our study. The best "model" to study human disease is the patient, but in AF, the tissues in which the molecular changes occur that confer and sustain AF are not readily accessible or can only be obtained in the latter stages of the disease process. The difficulties for human research are balanced by the challenges of animal models in which a single or even several animal models of AF can never be representative of all forms of AF. This model of AF relies on the heterogeneous expression of a mutant $\text{Nav}1.5$, which confers increased persistent Na^+ current and heterogeneous prolongation of the APD. Although increased persistent Na^+ current in atrial cardiomyocytes is associated with AF in humans (2), we cannot conclude that

the APD dispersion observed in the LA of humans with AF is due to heterogeneous persistent Na^+ current. Furthermore, although the ex vivo use of ATX-II to increase APD and reduce APD heterogeneity was effective to attenuate the inducibility of AF, its use in vivo is not a viable therapeutic strategy. Ranolazine is FDA-approved for chronic angina, but is not approved for AF, although recent trials suggest efficacy (28).

In summary, these studies experimentally demonstrate that dispersion of the APD is absolutely required for perpetuation of AF in a mouse model caused by increased persistent Na^+ current. Rotors and wave-breaks, the electrophysiological basis for AF, are anchored to the regions of greatest APD dispersion. Reducing the heterogeneity of the APD, even in the presence of increased EADs, prevented the induction of rotors and wavebreaks, and thereby was anti-fibrillatory. Since spatial APD heterogeneity is present in humans with AF, we propose that identifying regions of APD inhomogeneity may be a novel approach to target key arrhythmic drivers of AF.

MATERIAL AND METHODS

Animals: All animal experiments were performed according to NIH guidelines. The Institutional Animal Care and Use Committee at Columbia University approved all animal experiments. Both male and female genders, between 3-12 months of age, of the F1759A-Nav1.5 TG mice line (5) and littermate controls were used in this study.

Human studies: Patients undergoing ablation for AF at Columbia University-NY Presbyterian Hospital were enrolled after obtaining informed consent. The study was approved by the Columbia University Institutional Review Board. A deflectable 7 Fr MAP catheter (MedFact Engineering, Löracch, Germany) was used. Unipolar data acquisition was performed during atrial pacing at a cycle length of 500 ms. Signal filtering was 0.05-500 Hz (MAPs), 30-500Hz (other cardiac signals) and 0.05-100Hz (ECG). APD was measured at 90% repolarization during atrial pacing at a cycle length of 500 ms (120 beats per minute) using customized Matlab software. Three-dimensional electro-anatomical voltage maps of the LA were obtained using CARTO3 (Biosense Webster, Irvine, CA) or EnSite Precision (Abbott, Lake Bluff, IL).

Cellular Electrophysiology: Atrial cardiomyocytes and cellular electrophysiology was performed as described (5). Membrane currents from non-contracting rod-shaped atrial cardiomyocytes with clear striations were measured using whole-cell-patch-clamp with a MultiClamp 700B amplifier and pCLAMP software (Molecular Devices). The pipette resistance was 0.4-1.0 M Ω in order to minimize voltage clamp error. The cell capacitance currents were compensated. Series resistances were compensated at 60%. The leak current was subtracted using a P/4 protocol. The intracellular pipette solution contained (in mM): 5 NaCl, 20 CsCl, 115 CsF, 10 HEPES, and 10 BAPTA (pH 7.4) titrated with CsOH. For persistent Na⁺ current determinations, the bath solution contained (in mM): 100 NaCl, 45 TEA-Cl, 10 HEPES, 1 MgCl₂, 0.25 CaCl₂, and 5 glucose (pH 7.4) titrated

with CsOH. In voltage clamp mode cell membrane potential was held at -110 mV and stepped to -30 mV for 190 ms in the absence and in the presence of ranolazine (200-500 μ M). The mean values of the currents during the last 10 ms of the 190-ms were measured. The difference of these values – “ranolazine-sensitive” current - was used as a measure of persistent Na⁺ current and later normalized to cell capacitance. Peak Na⁺ current density was determined using 5 mM NaCl in the bath solution. Lidocaine (3 mM) was superfused in the bath solution to determine the lidocaine-resistant current.

Confocal Microscopy and Immunofluorescence: Isolated atrial cardiomyocytes were fixed for 15 minutes in 4% paraformaldehyde. Indirect fluorescence was performed using 1:200 rabbit anti-FLAG antibody (Product #F7425, Sigma-Aldrich) and 1:200 FITC-labeled goat anti-rabbit antibody (Product #F2555, Sigma-Aldrich). Images were acquired using a confocal microscope.

Optical mapping data acquisition and processing: Optical mapping was performed (5) using a complementary metal-oxide-semiconductor (CMOS) camera (MICAM Ultima, SciMedia). Movies were acquired at 1000 f/s for 4-5 sec, with 100 x 100 pixel resolution (0.095 mm per pixel). Images were processed using custom software, PV-WAVE (Precision Visuals - Workstation Analysis and Visualization Environment, Visual Numerics, Inc) (30). Dominant frequency (DF) and phase maps were obtained in AF, and APD and conduction velocity maps were obtained with atrial pacing at 10-Hz. Average APD, maximum APD and APD dispersion ($APD_{max} - APD_{min}$) were calculated for the whole atria and compared between the regions of highest singularity point density (SPD) to a neighboring 10 x 10 pixel area (30). High APD gradients were defined as regions where the difference between a long APD and a neighboring short APD within a 10 x 10 pixel area is greatest. Rotational activity of at least one cycle was classified as a rotor (30). Singularity point density maps were created by overlaying the distribution of singularity points

from the phase movie for ~ 4.1 secs. The high singularity point density regions were defined as singularity point density $>30\%$ compared to surrounding pixels (30). Pacing-induced AF was assessed by 3 attempts of burst pacing at twice the excitation threshold of the left atrium (20-Hz, amplitude 0.5–2.0 mA, 5 ms). SEA-0400 (Chemscene Chemicals, Monmouth, NJ), ranolazine (Alomone, Jerusalem, Israel), anemone toxin II (Sigma, St Louis, MO) and digoxin (West-ward Pharmaceutical, London, UK) were retrograde perfused via the aortic cannula.

Computational Modeling: A cellular automaton was used to model atrial fibrillatory activity (16). A grid consisting of 576×576 nodes was used for analysis. The distance between nodes was set at 1 mm, and the time step was 2 ms. Each node was programmed to one of three states: (1) activating, (2) recovering from activation, such as being in the refractory state, or (3) recovered from activation and excitable. State 1 was set to 2 ms, while state 2 — the refractory period or APD, was varied throughout the grid. The conduction velocity for wavefront propagation was set to 0.5 mm/ms along the vertical axis and 0.25 mm/ms along the horizontal axis (anisotropic ratio of 2:1).

Statistical Analysis: Group data are presented as mean \pm SEM. Statistical comparisons between the groups were tested using an unpaired two tailed Student's *t*-test and ANOVA tests for multiple comparisons. A *P* value <0.05 was considered statistically significant. All statistical analyses were performed with Prism 6.0.

Study Approval: Human subjects research was approved by the Columbia University Institutional Review Board, Columbia University Human Research Protection Office, 154 Haven Ave, 1st

Floor, New York, New York 10032. All subjects provided informed consent prior to their participation in the study.

Acknowledgments: The authors thank Dr. Igor Efimov (George Washington University) for generous technical assistance on the optical imaging experiments and analysis. The authors thank Dr. José Jalife (University of Michigan) and Dr. James Coromilas (Robert Wood Johnson Medical School and Rutgers Biomedical and Health Sciences) for helpful discussions and suggestions. We thank Sadiq Khan, Kristin Pallister and Dr. Pierre Nauleau for technical assistance. We thank Dr. Angelo Biviano for help with monophasic action potential recordings.

Author contributions: UMA, SOM, ARM and EW designed the study. EW, UMA, JA, AK, SZ, SM, JB, DR, AG, MW, VI, DS, EJC and LY performed experiments and collected the data. UMA, HG, ARM, SOM and EW analyzed the data. UMA, SOM, and EW wrote the manuscript.

Sources of Funding: The research was supported by NHLBI R01 HL122967 and R01HL123483 to SOM, and a gift from the Iazard family to E.W. E.W. was supported by NIH K08HL122526, the Louis V. Gerstner, Jr. Scholars Program, the Esther Aboodi Endowed Professorship at Columbia University and the M. Irène Ferrer Scholar Award from the Foundation of Gender Specific Medicine.

Disclosures: EYW previously received financial compensation for speaking at Abbott and Medtronic teaching symposia not related to the research in this manuscript. ARM is the founding scientist and chair of the SAB of ARMGO Pharma, Inc. which is targeting leaky RyR channels for

treatment of cardiovascular and skeletal muscle disorders including AF, but not related to the research in this manuscript. Both A.R.M and Columbia University own equity in ARMGO. The other authors have no conflicts of interest nor disclosures to declare.

REFERENCES

1. Moss AJ, and Kass RS. Long QT syndrome: from channels to cardiac arrhythmias. *J Clin Invest*. 2005;115(8):2018-24.
2. Sossalla S, Kallmeyer B, Wagner S, Mazur M, Maurer U, Toischer K, et al. Altered Na(+) currents in atrial fibrillation effects of ranolazine on arrhythmias and contractility in human atrial myocardium. *J Am Coll Cardiol*. 2010;55(21):2330-42.
3. Toischer K, Hartmann N, Wagner S, Fischer TH, Herting J, Danner BC, et al. Role of late sodium current as a potential arrhythmogenic mechanism in the progression of pressure-induced heart disease. *J Mol Cell Cardiol*. 2013;61:111-22.
4. Signore S, Sorrentino A, Borghetti G, Cannata A, Meo M, Zhou Y, et al. Late Na(+) current and protracted electrical recovery are critical determinants of the aging myopathy. *Nat Commun*. 2015;6:8803.
5. Wan E, Abrams J, Weinberg RL, Katchman AN, Bayne J, Zakharov SI, et al. Aberrant sodium influx causes cardiomyopathy and atrial fibrillation in mice. *J Clin Invest*. 2016;126(1):112-22.
6. Wang YL, Liu X, Zhang Y, Jiang WF, Zhou L, Qin M, et al. Optimal endpoint for catheter ablation of longstanding persistent atrial fibrillation: A randomized clinical trial. *Pacing Clin Electrophysiol*. 2017.
7. Narayan SM, Krummen DE, Shivkumar K, Clopton P, Rappel WJ, and Miller JM. Treatment of atrial fibrillation by the ablation of localized sources: CONFIRM (Conventional Ablation for Atrial Fibrillation With or Without Focal Impulse and Rotor Modulation) trial. *J Am Coll Cardiol*. 2012;60(7):628-36.
8. Cochet H, Dubois R, Yamashita S, Al Jefairi N, Berte B, Sellal JM, et al. Relationship Between Fibrosis Detected on Late Gadolinium-Enhanced Cardiac Magnetic Resonance and Re-Entrant Activity Assessed With Electrocardiographic Imaging in Human Persistent Atrial Fibrillation. *JACC Clin Electrophysiol*. 2018;4(1):17-29.
9. Chrispin J, Gucuk Ipek E, Zahid S, Prakosa A, Habibi M, Spragg D, et al. Lack of regional association between atrial late gadolinium enhancement on cardiac magnetic resonance and atrial fibrillation rotors. *Heart Rhythm*. 2016;13(3):654-60.
10. Sohns C, Lemes C, Metzner A, Fink T, Chmelevsky M, Maurer T, et al. First-in-Man Analysis of the Relationship Between Electrical Rotors From Noninvasive Panoramic Mapping and Atrial Fibrosis From Magnetic Resonance Imaging in Patients With Persistent Atrial Fibrillation. *Circ Arrhythm Electrophysiol*. 2017;10(8).
11. Campbell K, Calvo CJ, Mironov S, Herron T, Berenfeld O, and Jalife J. Spatial gradients in action potential duration created by regional magnetofection of hERG are a substrate for wavebreak and turbulent propagation in cardiomyocyte monolayers. *J Physiol*. 2012;590(Pt 24):6363-79.
12. Seitz J, Bars C, Theodore G, Beurtheret S, Lellouche N, Bremond M, et al. AF Ablation Guided by Spatiotemporal Electrogram Dispersion Without Pulmonary Vein Isolation: A Wholly Patient-Tailored Approach. *J Am Coll Cardiol*. 2017;69(3):303-21.
13. Qu Z, Garfinkel A, Chen PS, and Weiss JN. Mechanisms of discordant alternans and induction of reentry in simulated cardiac tissue. *Circulation*. 2000;102(14):1664-70.
14. Al Abed A, Lovell NH, and Dokos S. Local Heterogeneous Electrical Restitution Properties of Rabbit Atria. *J Cardiovasc Electrophysiol*. 2016;27(6):743-53.
15. Franz MR. Current status of monophasic action potential recording: theories, measurements and interpretations. *Cardiovasc Res*. 1999;41(1):25-40.

16. Ciaccio EJ, Peters NS, and Garan H. Effects of refractory gradients and ablation on fibrillatory activity. *Comput Biol Med.* 2018;95:175-87.
17. Sanbe A, Gulick J, Hanks MC, Liang Q, Osinska H, and Robbins J. Reengineering inducible cardiac-specific transgenesis with an attenuated myosin heavy chain promoter. *Circ Res.* 2003;92(6):609-16.
18. Valencik ML, and McDonald JA. Codon optimization markedly improves doxycycline regulated gene expression in the mouse heart. *Transgenic Res.* 2001;10(3):269-75.
19. McNulty MM, Edgerton GB, Shah RD, Hanck DA, Fozzard HA, and Lipkind GM. Charge at the lidocaine binding site residue Phe-1759 affects permeation in human cardiac voltage-gated sodium channels. *J Physiol.* 2007;581(Pt 2):741-55.
20. Narayan SM, Franz MR, Clopton P, Pruvot EJ, and Krummen DE. Repolarization alternans reveals vulnerability to human atrial fibrillation. *Circulation.* 2011;123(25):2922-30.
21. Du C, Zhang Y, El Harchi A, Dempsey CE, and Hancox JC. Ranolazine inhibition of hERG potassium channels: drug-pore interactions and reduced potency against inactivation mutants. *J Mol Cell Cardiol.* 2014;74:220-30.
22. Catterall WA, Cestele S, Yarov-Yarovoy V, Yu FH, Konoki K, and Scheuer T. Voltage-gated ion channels and gating modifier toxins. *Toxicol.* 2007;49(2):124-41.
23. Saha M, Roney CH, Bayer JD, Meo M, Cochet H, Dubois R, et al. Wavelength and Fibrosis Affect Phase Singularity Locations During Atrial Fibrillation. *Front Physiol.* 2018;9:1207.
24. Varela M, Colman MA, Hancox JC, and Aslanidi OV. Atrial Heterogeneity Generates Re-entrant Substrate during Atrial Fibrillation and Anti-arrhythmic Drug Action: Mechanistic Insights from Canine Atrial Models. *PLoS Comput Biol.* 2016;12(12):e1005245.
25. Remme CA. Cardiac sodium channelopathy associated with SCN5A mutations: electrophysiological, molecular and genetic aspects. *J Physiol.* 2013;591(17):4099-116.
26. Benito B, Brugada R, Perich RM, Lizotte E, Cinca J, Mont L, et al. A mutation in the sodium channel is responsible for the association of long QT syndrome and familial atrial fibrillation. *Heart Rhythm.* 2008;5(10):1434-40.
27. Scirica BM, Morrow DA, Hod H, Murphy SA, Belardinelli L, Hedgepeth CM, et al. Effect of ranolazine, an antianginal agent with novel electrophysiological properties, on the incidence of arrhythmias in patients with non ST-segment elevation acute coronary syndrome: results from the Metabolic Efficiency With Ranolazine for Less Ischemia in Non ST-Elevation Acute Coronary Syndrome Thrombolysis in Myocardial Infarction 36 (MERLIN-TIMI 36) randomized controlled trial. *Circulation.* 2007;116(15):1647-52.
28. Reiffel JA, Camm AJ, Belardinelli L, Zeng D, Karwatowska-Prokopczuk E, Olmsted A, et al. The HARMONY Trial: Combined Ranolazine and Dronedarone in the Management of Paroxysmal Atrial Fibrillation: Mechanistic and Therapeutic Synergism. *Circ Arrhythm Electrophysiol.* 2015;8(5):1048-56.
29. Kondo M, Nesterenko V, and Antzelevitch C. Cellular basis for the monophasic action potential. Which electrode is the recording electrode? *Cardiovasc Res.* 2004;63(4):635-44.
30. Yamazaki M, Avula UM, Bandaru K, Atreya A, Boppana VS, Honjo H, et al. Acute regional left atrial ischemia causes acceleration of atrial drivers during atrial fibrillation. *Heart Rhythm.* 2013;10(6):901-9.

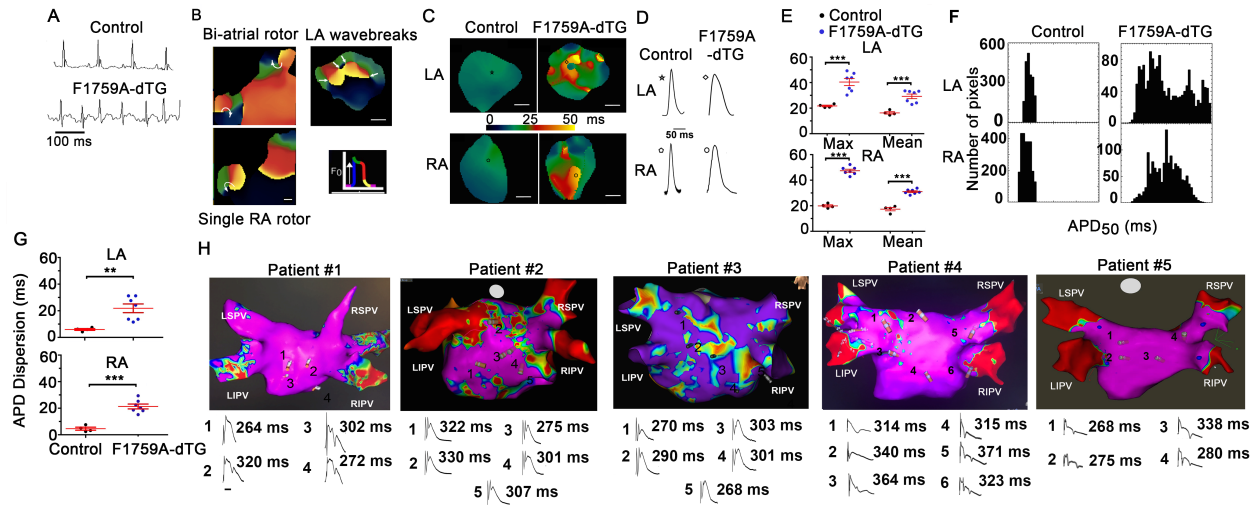


Figure 1 Inhomogeneity of action potential duration in mice and humans with atrial fibrillation. (A) Representative limb lead surface electrocardiograms of isoflurane-anesthetized littermate control mouse in sinus rhythm (top row) and of F1759A-dTG mouse in AF (lower row). (B) Representative snapshots from phase movies of Langendorff-perfused F1759A-dTG hearts demonstrating simultaneous rotors in the right atrium (RA) and left atrium (LA), a predominant rotor in the RA, and wavebreaks and fibrillatory conduction in the LA. (C-D) Representative optical APD maps (C) and optical action potential tracings (D) from littermate control and F1759A-dTG mice. APD maps (pacing at 10-Hz) for F1759A-dTG were obtained after hyperkalemia-induced conversion to sinus rhythm. The circle marks the region corresponding to the optical action potential tracings in (D). Scale bar = 1 mm. (E) Graph showing maximal (max) and mean APD₅₀ in LA and RA of littermate control (N=4) and F1759A-dTG mice (N=7). Mean \pm SEM. *** $P < 0.001$; t-test. (F) Representative all-points histograms of APD. (G) Graphs of APD₅₀ dispersion. Mean \pm SEM for littermate control and F1759A-dTG mice ** $P < 0.01$; *** $P < 0.01$; t-test. (H) Electro-anatomical voltage map (upper) and MAP recordings in sinus rhythm (lower) with APD₉₀ measurement for the corresponding regions for 5 patients undergoing AF ablation. For electro-anatomical voltage map, red color (0.2 mV) is indicative of low voltage area consistent with scarred tissue and purple (0.5-1.0 mV) is indicative of normal healthy tissue.

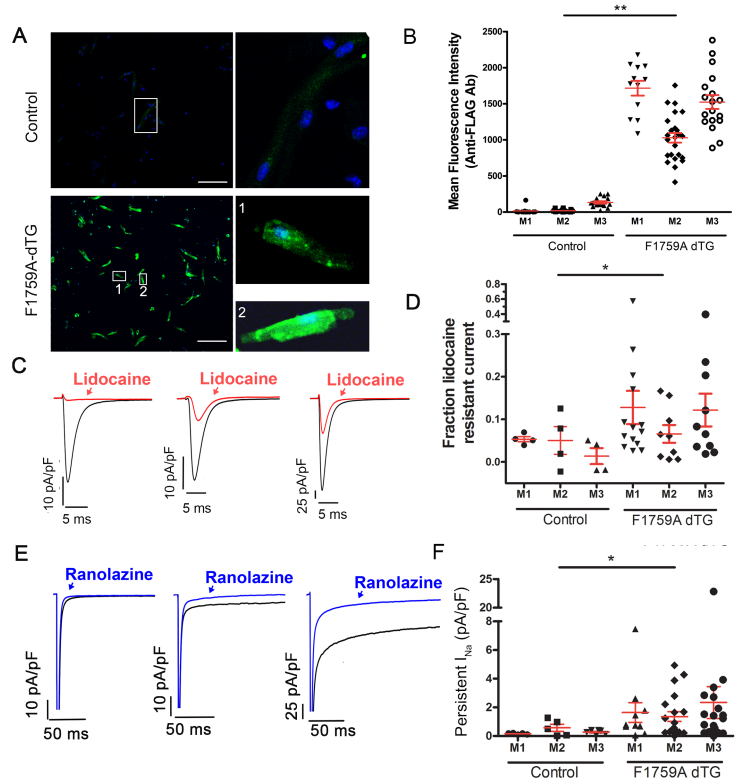


Figure 2 Inhomogeneity of TG Nav1.5 expression and persistent Na⁺ current in F1759A-dTG mice. (A) Representative immunofluorescent images of atrial cardiomyocytes isolated from littermate control mice and F1759A-dTG mice. Atrial cardiomyocytes were permeabilized and incubated with or without anti-FLAG antibody and with FITC-conjugated secondary antibody. Images were obtained with confocal microscopy at 20X (left) and 40X magnification (right). Scale bar =100 μm. (B) Graph quantifying immunofluorescent intensity using ImageJ. Mean ± SEM. *** $P < 0.001$; t -test, $N=3$ mice for each group, control and F1759A-dTG, M1= Mouse 1, M2= Mouse 2, M3= Mouse 3. (C) Exemplar whole cell Na⁺ current (I_{Na}) traces of atrial cardiomyocytes isolated from F1759A-dTG mice. Whole cell current traces were recorded with 5 mM Na⁺ in both extracellular and intracellular solutions, in the absence (black) and presence (red) of 3 mM lidocaine. (D) Fraction of lidocaine-resistant current for littermate control, Mean ± SEM, $N=3$ mice for each group, control and F1759A-dTG, M1= Mouse 1, M2= Mouse 2, M3= Mouse 3. (E) Exemplar whole cell Na⁺ current traces designed to assess persistent I_{Na} using a 190-ms depolarization from a holding potential of -110 to -30 mV in the absence (black) and presence (blue) of 500 μM ranolazine; intracellular solution contained 5 mM Na⁺ and extracellular solution contained 100 mM Na⁺ was used in the. $N=3$ mice, $n= 54$ cardiomyocytes. (F) Graph of extent of persistent I_{Na}. Mean ± SEM. $N=3$ mice for each group, control and F1759A-dTG, M1= Mouse 1, M2= Mouse 2, M3= Mouse 3. *** $P < 0.001$; t -test.

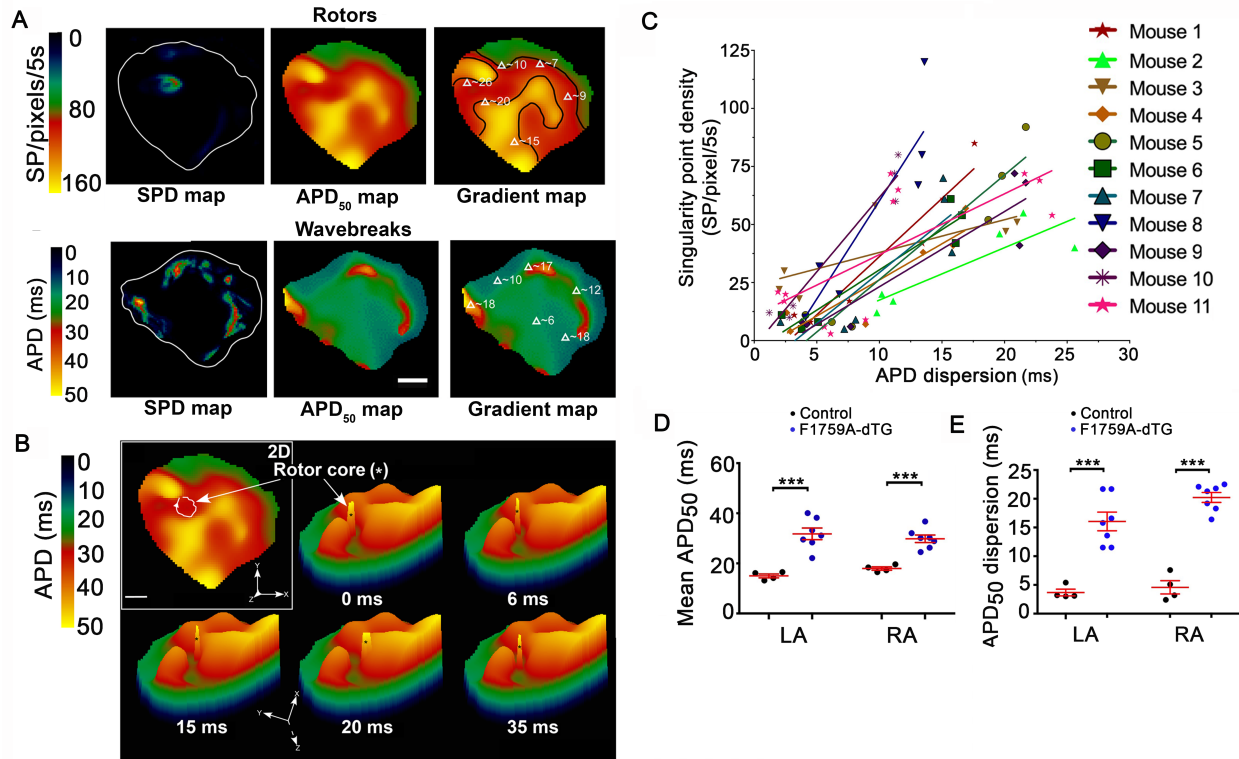


Figure 3 Rotors are anchored in regions of high spatial action potential duration inhomogeneity. (A) Representative singularity point density (SPD) maps and corresponding APD₅₀ maps (middle) of single rotor (upper) and wavebreaks (lower) from F1759A-dTG mice. In the gradient APD₅₀ map (right), differences in APD₅₀ between adjacent segments are shown on the contoured gradient map (Δ in milliseconds (ms)). Note alignment of high density of singularity points and dispersion of APD. Scale bar = 1 mm. (B) Representative 2-dimensional and 3-dimensional images of the APD₅₀ within the LA of a F1759A-dTG mouse. The positions of the rotor core at different time-points are overlaid on the APD₅₀ maps. The trajectory of the rotor core is delimited within the regions of high spatial APD gradients. (C) Scatter plot depicting correlation between APD dispersion and singularity point density. Lines are best fit. Mouse 1: $R^2=0.92$, $P < 0.01$; Mouse 2: $R^2=0.75$, $P < 0.05$; Mouse 3: $R^2=0.56$, $P = 0.09$; Mouse 4: $R^2=0.81$, $P < 0.05$; Mouse 5: $R^2=0.91$, $P < 0.01$; Mouse 6: $R^2=0.90$, $P < 0.01$; Mouse 7: $R^2=0.72$, $P < 0.05$; Mouse 8: $R^2=0.81$, $P < 0.05$; Mouse 9: $R^2=0.85$, $P < 0.01$; Mouse 10: $R^2=0.95$, $P < 0.001$; Mouse 11: $R^2=0.54$, $P < 0.01$. (D) Graph showing mean APD₅₀ at the maximal singularity point density position in the left and right atria of F1759A-dTG mice. Mean \pm SEM. *** $P < 0.001$ by t -test. (E) Graph of APD₅₀ dispersion at the maximal singularity point density position in the left and right atria of F1759A-dTG mice. Mean \pm SEM. *** $P < 0.001$ by t -test.

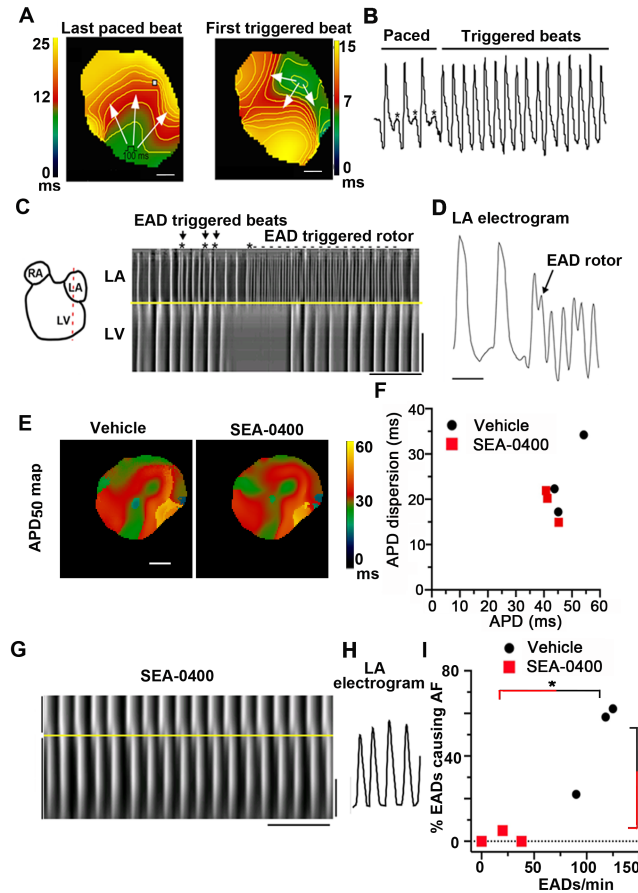


Figure 4 Triggered activity is required for initiation and perpetuation of atrial fibrillation in F1759A-dTG mice. (A) Isochronal map of atrial paced beat and first-triggered beat. (B) Electrogram shows triggered beats after atrial pacing at 10-Hz. Scale bar = 1 mm. (C-D) Time space plots of left atrium and left ventricle (LV) during 10-Hz atrial pacing. EAD's are marked by "*" Horizontal scale bar = 500 ms. Vertical scale bar = 2.5 mm. Single pixel electrograms (D) showing EADs, and rotor. Scale bar = 100 ms. (E) APD₅₀ map of Langendorff-perfused F1759A-dTG heart after conversion to sinus rhythm before (vehicle) and after 3 μ M SEA-0400. Scale bar = 1 mm. (F) Graph depicting relationship between APD and APD dispersion before (vehicle) and after SEA-0400 perfusion. N=3. $P = 0.37$ by t-test. (G-H) Time space plots of left atrium and left ventricle (LV) during 10-Hz atrial pacing after SEA-0400. Horizontal scale bar = 500 ms. Vertical scale bar = 2.5 mm. Single pixel electrograms (H) showing normal rhythm without EADs or rotors. (I) Graph depicting relationship between number of EADs/min and % EADs causing AF before (vehicle) and after SEA-0400 perfusion. N=3. $P < 0.05$ by t-test for both EADs/min and % EADs causing AF.

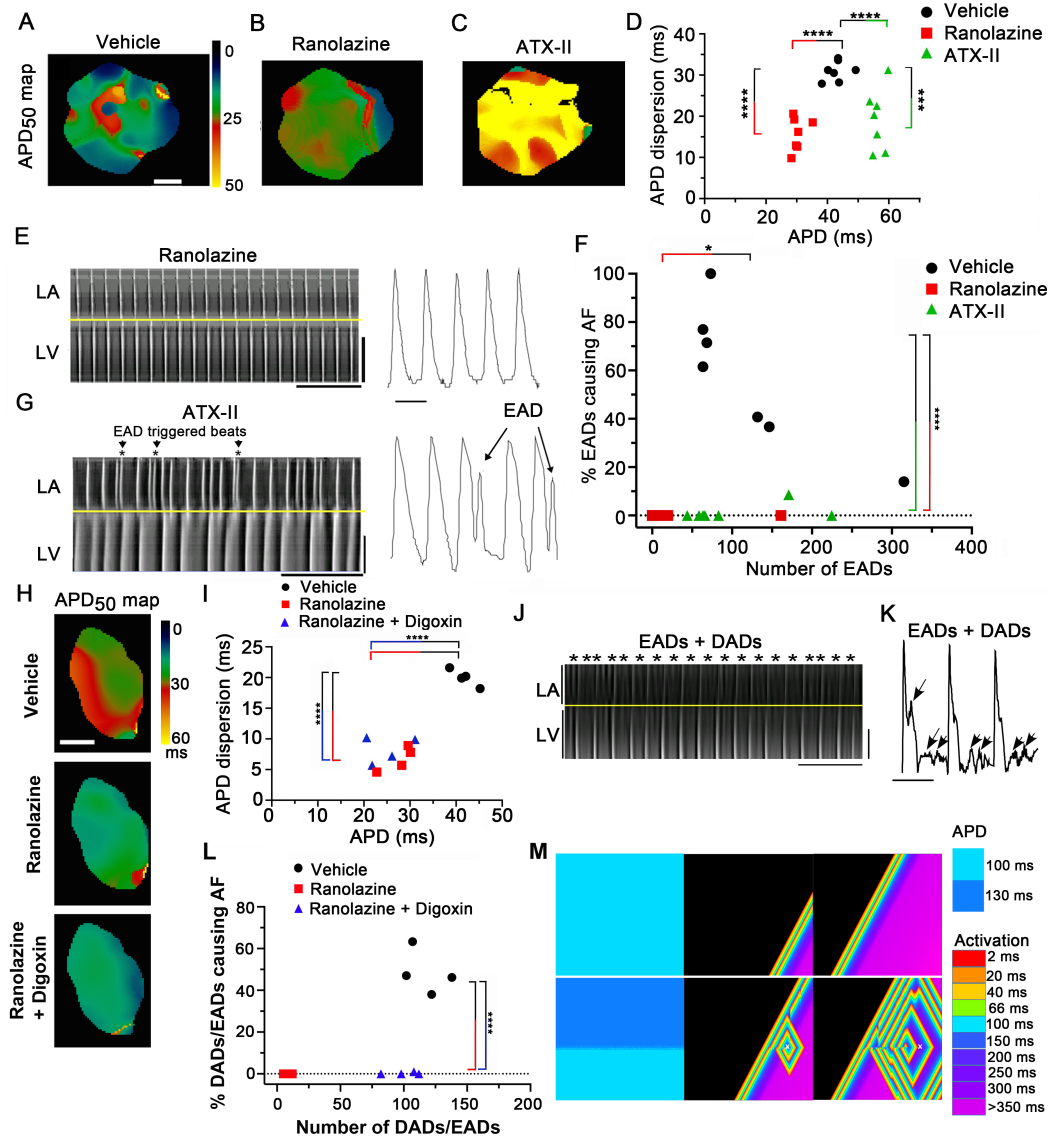


Figure 5 Inhomogeneity of the action potential duration is required for atrial fibrillation in F1759A-dTG mice. (A-C) Representative APD₅₀ maps in sinus rhythm before (vehicle), after 500 μ M ranolazine and after 20 nM anemone toxin II (ATX-II). Scale bar = 1 mm. (D) Graph depicting relationship between APD and APD dispersion before (vehicle) and after either 500 μ M ranolazine or 20 nM ATX-II. ***, $P < 0.001$; ****, $P < 0.0001$ by Anova and Dunnett's multiple comparison test. The color and direction of the brackets indicate the pair of comparisons. (E) Representative time space plot of LA and left ventricle (LV) during 10-Hz atrial pacing after 500 μ M ranolazine. Scale bar = 500 ms. (F) Graph depicting relationship between number of EADs/min and % EADs causing AF before (vehicle) and after either ranolazine or ATX-II. *, $P < 0.05$ and ****, $P < 0.0001$ by Anova and Dunnett's multiple comparison test. The color and direction of the brackets indicate the pair of comparisons. (G) Representative time space plot of left atrium and left ventricle (LV) during 10-Hz atrial pacing after 20 nM ATX-2. EAD's are marked by "*" Horizontal scale bar = 500 ms. Vertical scale bar = 2.5 mm. Electrogram shows EADs, scale bar = 100 ms. (H) Representative APD₅₀ maps in sinus rhythm before (vehicle), after 500 μ M ranolazine and after ranolazine and 0.9 μ M digoxin. (I) Graph depicting relationship between APD and APD dispersion

before (vehicle) and after either 500 μ M ranolazine or 500 μ M ranolazine + 0.9 μ M digoxin ***, $P < 0.001$; ****, $P < 0.0001$ by Anova and Dunnett's multiple comparison test. The color and direction of the brackets indicate the pair of comparisons. **(J)** Representative time space plot of left atrium and left ventricle (LV) during 10-Hz atrial pacing after ranolazine and digoxin. After-depolarizations are marked by "*". **(K)** Electrogram shows EADs and DADs. **(L)** Graph depicting relationship between number of after-depolarization/min and % after-depolarizations causing AF before (vehicle) and after either ranolazine or ranolazine and digoxin. The color and direction of the brackets indicate the pair of comparisons. **(M)** Automaton-simulation of fibrillatory activity in atrial tissue. Upper, A uniform APD gradient of 100 ms was imposed. Lower, Two APDs were imposed: 100 ms and 130 ms. Electrical activation was initiated by a S1-S2 pulse with 84 ms coupling interval from the lower right-hand grid corner (node set to state 1 for each pulse- see Methods). No reentry was seen in a homogeneous uniform gradient. In the nonuniform simulation, activation by a S1-S2 pulse caused fibrillatory activity in the form of rotors at the boundary between the two APD gradients of 100 and 130 ms.